chemosensors

Article

A Facile Solid-Phase Synthesis of Scandium-Modified Carbon Dots for Fluorescent Sensing of Cu^{2+}

Yalei Dong [1,†], Wei Song [2,3,†], Jing Hu [4,*] and Cuiling Ren [2,*]

[1] National Institutes for Food and Drug Control, Beijing 100050, China; dongyalei@nifdc.org.cn
[2] Department of Chemistry, Key Laboratory of Nonferrous Metal Chemistry and Resources Utilization of Gansu Province, Lanzhou University, Lanzhou 730000, China; songwei@sioc.ac.cn
[3] Shanghai Institute of Organic Chemistry, Chinese Academy of Sciences, Shanghai 200032, China
[4] Suzhou Key Laboratory for Nanophotonic and Nanoelectronic Materials and Its Devices, School of Materials Science and Engineering, Suzhou University of Science and Technology, Suzhou 215009, China
* Correspondence: hujlina@usts.edu.cn (J.H.); rencl@lzu.edu.cn (C.R.); Tel.: +86-931-8912763 (C.R.)
† These authors contribute equally to this work.

Abstract

Scandium-modified carbon dots (Sc-oCDs) were synthesized in this work through a solid-phase approach. The prepared Sc-oCDs exhibited excitation-independent emission properties, as well as photostability against pH, ionic strength, and UV irradiation. Their fluorescence quantum yields significantly exceeded those of unmodified counterparts, confirming effective Sc modification. The Sc-oCDs also possessed upconversion fluorescence at 542 nm with 980 nm excitation. Additionally, the as-prepared Sc-oCDs functioned as an effective fluorescent sensor for Cu^{2+}, demonstrating selective fluorescence quenching. A linear correlation was observed between the quenching efficiency and Cu^{2+} concentration from 1 to 600 μM, achieving a detection limit of 0.167 μM. Operating via dynamic quenching, this sensing system achieved highly selective and rapid (<1 min) detection of Cu^{2+}, enabling sensitive Cu^{2+} monitoring in aqueous samples.

Keywords: scandium-modified carbon dots; solid-phase synthesis; upconversion; Cu^{2+}; dynamic quenching

check for updates

Received: 2 October 2025
Revised: 7 December 2025
Accepted: 8 December 2025
Published: 11 December 2025

Citation: Dong, Y.; Song, W.; Hu, J.; Ren, C. A Facile Solid-Phase Synthesis of Scandium-Modified Carbon Dots for Fluorescent Sensing of Cu^{2+}. *Chemosensors* **2025**, *13*, 430. https://doi.org/10.3390/chemosensors13120430

Copyright: © 2025 by the authors. Licensee MDPI, Basel, Switzerland. This article is an open access article distributed under the terms and conditions of the Creative Commons Attribution (CC BY) license (https://creativecommons.org/licenses/by/4.0/).

1. Introduction

Carbon dots (CDs) are a class of zero-dimensional carbon-based nanomaterials with sizes below 10 nm. They are renowned for their exceptional properties—including tunable fluorescence, facile modification, photostability, biocompatibility, and low toxicity [1,2]. These distinctive features enable them to be promising alternatives to semiconductor quantum dots and conventional organic dyes in various fields, including sensing, bioimaging, and drug delivery [3]. However, hurdles such as low near-infrared quantum yield, limited selectivity, and polydispersity persist. To address these limitations, heteroatom doping [4,5] (including nonmetallic atoms, e.g., N [6] and B [7], and metal ions, e.g., Fe [8] and Mg [9]) and co-doping [10,11] have proven effective in modulating electronic structures, enhancing fluorescence efficiency, and introducing new functionalities, thereby broadening their utility [12].

Rare earth elements (RE), owing to their distinctive 4f electron configurations, display abundant 4f–4f electronic transitions that span a broad spectral range. These transitions are marked by large Stokes shifts, narrow emission bands, and exceptionally long-lived excited states [13]. The remarkable properties of rare earth–carbon dots (RE-CDs) have led to their

growing prominence. These materials enable versatile applications, owing to energy exchange between RE^{3+} ions and CDs. CDs exhibit strong UV absorption and act as electron donors/acceptors, transferring energy to RE^{3+} ions, which are hard Lewis acids [14,15]. Consequently, RE-modified carbon dots have been prepared for luminescence [16,17], bioimaging [18,19], sensing [20,21], enzyme activity [22], and other applications. Scandium (Sc), the lightest transition metal and a highly valuable rare earth element [23], possesses unique properties due to its distinctive electron configuration. In nature, it exclusively exists in the +3 oxidation state (Sc^{3+}), which—with strong Lewis acidity and the smallest ionic radius among rare earth ions—exhibits exceptional complexation capabilities. Chen et al. [24] demonstrated that free Sc^{3+} ions significantly boosted the photocatalytic activity of carbon dots over a wide pH range for bio-nanozyme cascade colorimetric assays. Yang et al. [25] prepared Sc^{3+}-modified graphene quantum dots (GQDs), which effectively stabilized the photoluminescence of GQDs against quenching by heavy metal ions through surface modification. Inspired by the above research work, we envision that scandium modified carbon dots can be prepared to endow them with more excellent properties.

The solid-phase synthesis method, originally developed by Merrifield in 1984 for polypeptide synthesis, offered distinct advantages including operational simplicity, high yield, solvent-free conditions, and minimal purification requirements for products [26,27]. In recent decades, this methodology has found extensive applications in nanomaterial fabrication. Recent advances in solid-phase synthesis have enabled the fabrication of various doped quantum dots, including nitrogen-doped carbon dots with highly fluorescent [28], red dual-emissive nitrogen-doped variants [29], N,S-co-doped carbon dots [30], and Fe,N-co-doped nanozymes [31]. These studies demonstrate simplified preparation processes while achieving high fluorescence quantum yields and enhanced application performance.

Copper ions (Cu^{2+}), while essential in industrial and agricultural applications, become hazardous at elevated concentrations [32]. Their environmental persistence led to aquatic ecosystem disruption and bioaccumulation, while human exposure caused liver damage and neurological disorders [33]. The U.S. EPA (Environmental Protection Agency) has established a permissible level of 1.3 ppm for Cu^{2+} in drinking water [34]. The additional risk of Cu^{2+} leaching from plumbing systems into drinking water underscored the critical need for sensitive detection methods to ensure water safety and public health protection. Multiple analytical methods have been developed for detecting Cu^{2+} in diverse samples, such as atomic/molecular spectrophotometry [35], mass spectrometry [36], sensor technology [37], electrochemical [38], and chromatography [39]. Among various detection methods, QDs-based fluorescent sensors stand out due to their low cost, ease of miniaturization, and ability to provide rapid, quantitative results, making them highly valuable for monitoring Cu^{2+}.

Herein, scandium-modified carbon dots (Sc-oCDs) were papered by the solid-phase synthesis method, which does not need high temperatures or organic solvents. The experimental parameters for solid-phase synthesis of Sc-oCDs were systematically investigated, followed by material characterization. The superior optical properties of Sc-oCDs were also discussed, demonstrating enhanced fluorescence quantum yield along with both downconversion and upconversion photoluminescence (UCPL) capabilities. Moreover, the as-prepared Sc-oCDs exhibited selective fluorescence quenching on Cu^{2+}, as illustrated in Figure 1, supporting the application for Cu^{2+} detection in tap water and river water samples.

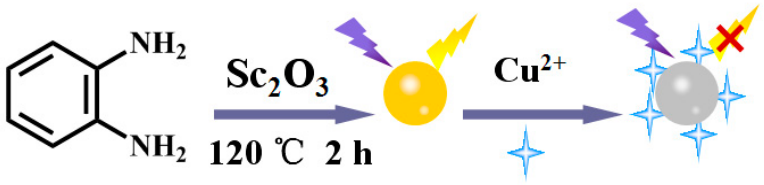


Figure 1. Solid-phase synthetic procedure of Sc-oCDs for Cu^{2+} detection. The blue star in the figure represents copper ion.

2. Materials and Methods

2.1. Chemicals

o-Phenylenediamine (oPD) and glycine were acquired from Tianjin Guangfu Chemical Reagents Co., Ltd. (Tianjin, China). Sc_2O_3 were obtained from J&K Scientific (Beijing, China). $MnCl_2$, $MgCl_2$, $BaCl_2$, $FeCl_3$, $FeCl_2$, $AlCl_3$, $CoCl_2$, $ZnCl_2$, $NiCl_2$, $CdCl_2$, $CrCl_3$, and $CuCl_2$ were bought from Sinopharm Chemical Reagent Co., Ltd. (Shanghai, China). Other reagents were analytical grade and employed as received. Ultrapure water was utilized throughout.

2.2. Instrumentation and Characterization

A fluorescence spectrophotometer (RF-5301PC, Shimadzu, Kyoto, Japan) was used to acquire fluorescence spectra. A double-beam UV-vis spectrophotometer (TU-1901, Beijing Purkine General Instrument Co., Ltd., Beijing, China) was employed to record absorption spectrum. The morphologies and size distribution of nanomaterials were characterized using transmission electron microscopy (TEM, Hitachi-600, Hitachi, Kyoto, Japan). Energy dispersive spectroscopy (EDS) characterization was performed using a scanning electron microscope (JSM-IT800, JEOL, Tokyo, Japan). FT-IR spectra were surveyed on an infrared spectrometer (Nicolet Nexus 670, Thermo Fisher Scientific Inc., Waltham, MA, USA). X-ray diffraction (XRD) patterns were obtained on an X-ray diffractometer with Cu Kα radiation (D/Max-2400, Rigaku, Tokyo, Japan). UCPL was carried out using a femtosecond pulsed laser excitation at 980 nm (Coherent Inc., Saxonburg, PA, USA) connecting an optical-multichannel analyzer (OMA) system. Inductively coupled plasma mass spectrometry (ICP-MS, Icap-Qc Ultimate 3000, Thermo Fisher Scientific Inc., Waltham, MA, USA) was used to detect the scandium content in the material in reference to the national standard (GB 5009.94-2012) [40]. The absolute fluorescence quantum yield was measured directly using a fluorescence spectrometer (FL920P, Edinburgh Instruments, Livingston, UK) equipped with an integrating sphere. Its time-correlated single-photon counting (TCSPC) system was employed to record the time-resolved fluorescence spectra.

2.3. Synthesis of Sc-oCDs

The synthesis method refers to a previous report [41]. Initially, 0.03 g oPD and 0.06 g Sc_2O_3 were first mixed in an agate mortar, ground thoroughly, and then transferred to a 50 mL stainless steel autoclave lined with Teflon. After reaction at 120 °C for 2 h, the autoclave was cooled naturally to room temperature. The resulting dark brown powder was dissolved in 5 mL of water. After centrifugation at 11,000 rpm for 15 min, the supernatant was collected and subjected to dialysis against ultrapure water for 24 h. Finally, the purified Sc-oCDs was further freeze-dried to obtain a deep dark brown powder. As comparison, the unmodified CDs (oCDs) were prepared using the same procedure as Sc-oCDs, except no Sc_2O_3 was added.

2.4. Fluorescence Quenching Experiments with Cu^{2+}

Briefly, 50 μL of a 0.02 mg/mL Sc-oCDs solution was combined with 2.92 mL of a Glycine–HCl buffer solution (10 mM, pH = 4.8). Immediately afterward, an aliquot of 30 μL of $CuCl_2$ solution, prepared at different concentrations (with the final Cu^{2+} concentrationvarying from 0 to 0.6 mM), was added. The fluorescence spectra of the reaction system were all recorded at an excitation wavelength (λ_{ex}) of 420 nm. For the selectivity experiments, the procedure remained identical, except interfering substances were substituted for Cu^{2+}.

2.5. Real Samples Analysis

Water samples from the Yellow River (Lanzhou section, Gansu Province, China) and tap water were collected and processed. All samples underwent centrifugation at 11,000 rpm for 15 min, followed by filtration of supernatant through membranes (0.45 μm) for later use.

Cu^{2+} detection in real samples followed the procedure in Section 2.4, except that the water sample solution was added instead of the $CuCl_2$ solution. Spike recovery tests were conducted at three concentration levels, each with three parallels.

3. Results and Discussion

3.1. Optimization of Synthesis Conditions for Sc-oCDs

Sc-oCDs were prepared by the solid-phase synthesis method as previously described [41]. To prepare Sc-oCDs with excellent optical properties, this work investigated the effects of synthesis temperature, time, and the mass ratio of Sc_2O_3 to oPD on the optical performance of the resulting products. Figure 2 displays the normalized fluorescence intensities of Sc-oCDs prepared under various conditions. Specifically, in Figure 2A, extending the reaction duration from 0.5 to 2 h maximizes the fluorescence intensity of the Sc-oCDs while further extension to 8 h causes a gradual decrease. This indicates that excessive carbonization time impairs fluorescence properties, so 2 h was determined to be the optimal reaction period. Fluorescence intensities of products prepared at different temperatures are shown in Figure 2B, peaking at 120 °C. The raw material ratio was further optimized. As Figure 2C shown, the strongest fluorescence occurred at an oPD:Sc_2O_3 mass ratio of 1:2, at which point the mass ratio of C to Sc provided by the precursors was 1:1. Thus, in subsequent experiments, Sc-oCDs synthesized under optimal reaction conditions (1:2 initial material ratio, reaction at 120 °C for 2 h) were used consistently.

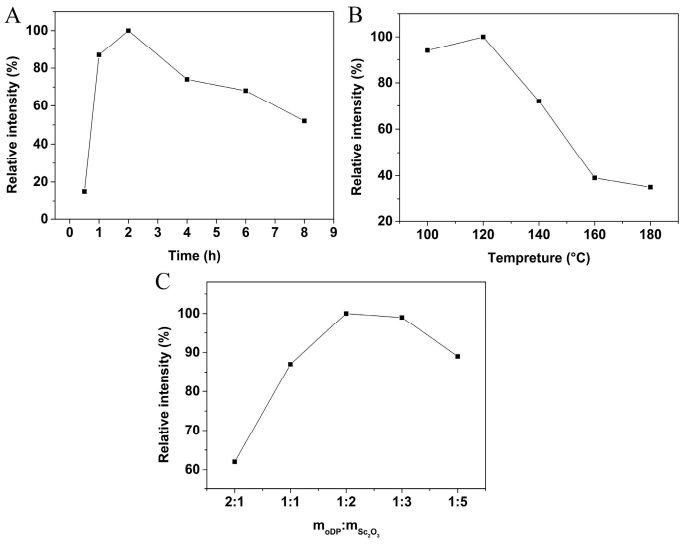


Figure 2. Normalized fluorescence intensity of Sc-oCDs synthesized under different (**A**) reaction times, (**B**) reaction temperatures, and (**C**) mass ratios of oPD and Sc_2O_3.

3.2. Characterization of Sc-oCDs

The morphology and size distribution of the prepared nanomaterials are characterized by TEM. As depicted in Figure 3A, the as-synthesized Sc-oCDs exhibits a nearly spherical shape, with their diameters varying from 4.0 to 8.0 nm. The corresponding size distribution analysis (Figure 3B) reveals that the mean size of Sc-oCDs was determined to be 6.0 ± 1.2 nm. The high-resolution TEM (HRTEM) image of Sc-oCDs reveals a well-resolved crystalline structure, with a lattice spacing of 0.23 ± 0.04 nm that matches the (100) diffraction plane of graphitic carbon [42].

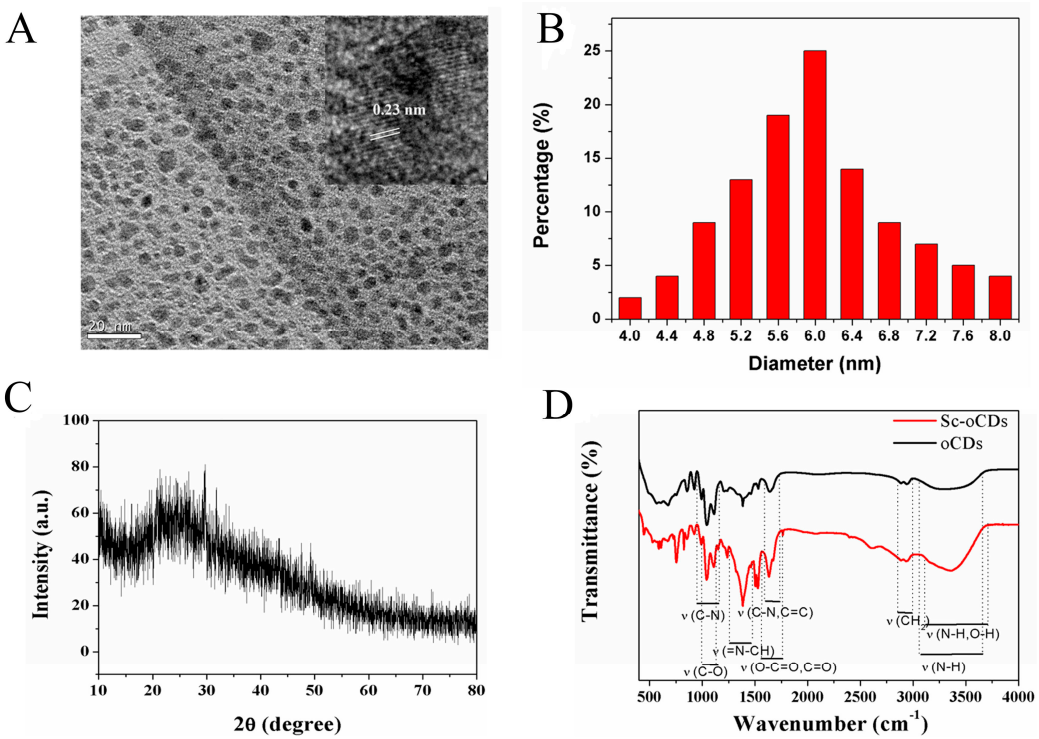


Figure 3. (**A**) TEM (inset is HRTEM) images, (**B**) size distribution histograms, (**C**) XRD pattern, and (**D**) FT-IR spectra of Sc-oCDs.

The typical XRD pattern of Sc-oCDs (Figure 3C) exhibits a broad diffraction peak in the range of 17° to 31°, which can be attributed to the (002) plane, confirming the graphitic structure of the Sc-oCDs [43]. In addition, the surface functional groups of Sc-oCDs are investigated using FT-IR spectroscopy. Figure 3D shows the characteristic broad absorption bands in the ranges of 3100–3600 cm^{-1}, which can be assigned to the stretching vibrations of O-H and N-H bonds [44]. The C-H stretching vibration peak appears in 2800–2900 cm^{-1}. The enhanced peaks between 1630 and 1680 cm^{-1} imply C–N and C=C bonds, thereby verifying that amino- and oxygen-containing functional groups are present on the Sc-oCDs' surface. The strong absorbance at 1385 cm^{-1} is assigned to the stretching vibration of =N-CH [45]. The peaks in the wavenumber range of 1043–1157 cm^{-1} correspond to the stretching vibrations of C–N. Moreover, compared with oCDs, the FT-IR bands at 1110–1157 cm^{-1} and 3100–3600 cm^{-1} appear sharper and broader. The deviations indicate that the amino and oxygen-containing groups in oPD interact with Sc_2O_3 during the synthesis of Sc-oCDs.

EDS analysis was also performed to verify the presence of Sc. As shown in the elemental mapping images (Figure S1), both C and Sc are homogeneously distributed throughout the materials, collectively confirming the successful modification and uniform dispersion of Sc. Due to the extremely low content of Sc, semi-quantitative analysis by EDS was not feasible. Therefore, we further conducted an ICP-MS experiment to quantify the scandium content in the material. Detailed descriptions of the experimental procedures

are provided in the Electronic Supplementary Information (ESI). The Sc content in the quantum dots is 0.26%, and the excessively low content is the reason why EDS cannot achieve quantitative analysis. According to existing reports in the literature, the content of rare earth elements in doped quantum dots is 0.53% [46], 1.52% [47] and 41.93% [48], and so on. The low content of Sc in Sc-oCDs precluded precise quantification by direct techniques such as EDS, representing a methodological limitation. The combined challenges of trace Sc amount and unclear modification mechanisms highlight the need for further in-depth study. Spectroscopic changes demonstrated that even trace Sc can modify optical properties and boost fluorescence.

3.3. Optical Properties of Sc-oCDs

The optical performance of Sc-oCDs was, respectively, characterized by UV-Vis and fluorescence spectra. In Figure 4A, the starting materials (oPD) and oCDs exhibit two comparable absorption peaks centered at 206 nm and 288 nm, respectively—both arising from the $\pi \rightarrow \pi^*$ electronic transition of C=C bonds. In comparison, three distinct absorption peaks were observed for Sc-oCDs at 206 nm, 258 nm and 421 nm, respectively. These differential absorption peaks between Sc-oCDs and oCDs/oPD suggest that Sc_2O_3 reacted with oPD under the experimental condition, which confirms that oCDs was successfully modified with Sc.

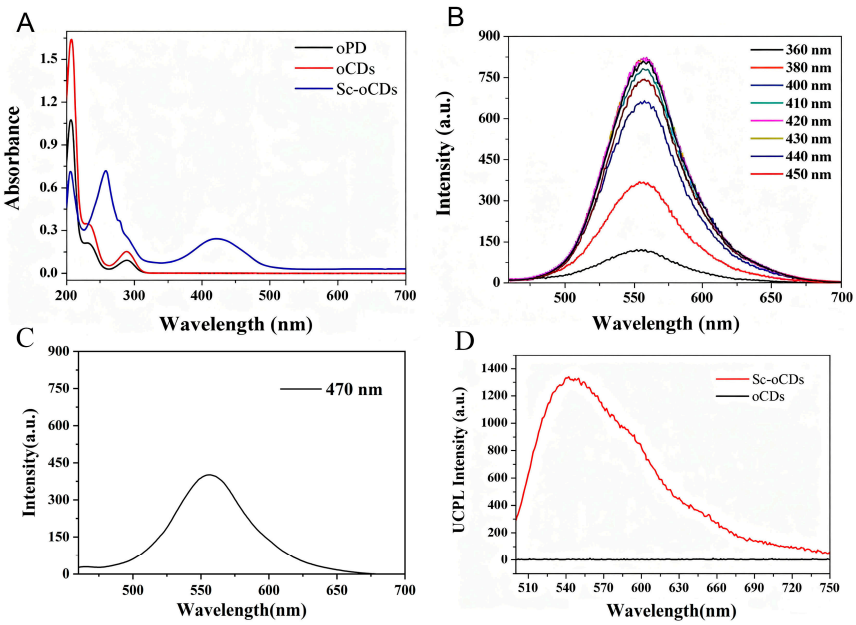


Figure 4. (**A**) UV/Vis absorption spectra of oPD, oCDs, and Sc-oCDs. (**B**) Fluorescent emission spectra of Sc-oCDs under different excitation wavelengths. (**C**) Fluorescent emission spectra of oCDs under 470 nm. (**D**) Emission spectra of Sc-oCDs and oCDs under excitation wavelengths of 980 nm.

Additionally, systematic investigations were conducted on the fluorescence emission spectra of Sc-oCDs in aqueous solution, using different excitation wavelengths. As shown in Figure 4B, the emission peaks remained unchanged as the excitation wavelengths varied from 360 nm to 450 nm. This excitation-independent emission behavior can be attributed to the relatively few surface defects and uniform particle size of Sc-oCDs [49], a finding that aligns with the results of TEM observations. Notably, its fluorescence intensity varied along with excitation wavelength, peaking at 420 nm. Consequently, this wavelength was chosen as the preferred excitation wavelength. For reference, unmodified oCDs without scandium were also prepared, and their fluorescence spectrum exhibited a maximum intensity at an excitation wavelength of 470 nm (Figure 4C). The observed shift in the

excitation wavelength and the enhancement of fluorescence intensity collectively indicate that Sc effectively modulated the optical properties of the material.

Based on the above fluorescence measurement results, the absolute fluorescence quantum yields (QY) of Sc-oCDs and oCDs were calculated, which was directly measured using the equipped integrating sphere module at the respective optimal wavelengths [50]. The results show that the QY of the Sc-oCDs is 11.3%, compared to 6.31% for oCDs. This enhanced fluorescence emission likely arose from Sc-induced changes to the chemical and electronic properties of carbon dots, confirming that scandium modification is an efficient approach to improve the QY of CDs [51]. Sc modification at a relatively low level in this study nonetheless resulted in improved optical properties of the quantum dots, indicating its potency even in small quantities.

Subsequent upconversion fluorescence spectra under 980 nm excitation (Figure 4D) reveal that Sc-oCDs emitted at 542 nm, whereas oCDs shows no fluorescence signal. This confirms that Sc endowed the carbon dots with upconversion fluorescence properties. The wavelength-independent phenomenon enabled Sc-oCDs to exhibit utility for both downconversion and upconversion properties, where unwanted autofluorescence can be avoided [52]. Based on the upconversion property of Sc-oCDs, we attempted to conduct MTT assays and cell imaging experiments using HeLa cells, just as we did in our previous research study [53]. However, the cell mortality rate led to unsatisfactory application results of this material in living cell samples. Currently, we are performing surface modification on this material to improve its biocompatibility and realize its application in living cells.

In addition, we investigated the optical stability of the resulting Sc-oCDs by examining the effects of ionic strength, light exposure, and pH on their fluorescence emission intensity. Firstly, the fluorescence intensities of Sc-oCDs in buffer solutions across a pH range of 3 to 12 are recorded. As presented in Figure S2A, the materials' fluorescence intensities stay largely stable across a pH range of 5–11. Then, Sc-oCDs display relatively stable fluorescence intensity (Figure S2B) even when the solution's ionic strength varies over a wide range, with NaCl concentration up to 1.0 M. These results suggest that the fluorescence properties of Sc-oCDs may not influenced by their surface states, which likely stem from the surface passivation caused by Sc modification and the starting materials [54]. Moreover, the fluorescence intensities of Sc-oCDs remain almost unaffected by ultraviolet light irradiation for 1 h (Figure S2C), suggesting their excellent photostability. Above all, such optical stability of the prepared Sc-oCDs renders them suitable for various biological applications.

3.4. Sensitivity of Sc-oCDs for the Detection of Cu^{2+}

To optimize the performance of Sc-oCDs for Cu^{2+} detection, this work investigates how buffer solution and pH influence the fluorescence quenching efficiency ($F_0 - F/F_0$), where F_0 and F represent the intensities of fluorescence for Sc-oCDs at 558 nm without and with Cu^{2+}, respectively. Figure S3A demonstrates that Cu^{2+} is capable of quenching the fluorescence emission in various buffer solutions, with the maximum quenching efficiency observed in glycine–HCl buffer. Figure S3B demonstrates the fluorescence quenching efficiency across pH conditions with Cu^{2+} (600 μM), peaking at pH 4.8. This is likely due to the enhanced affinity between Cu^{2+} and glycine via electrostatic interactions at this pH [55], so pH 4.8 was chosen as optimal. Moreover, the fluorescence of Sc-oCDs was completely quenched by Cu^{2+} within 1 min (Figure S3C), indicating that Sc-oCDs served as a fluorescent probe to enable the real-time tracking of Cu^{2+}.

The detection performance of Sc-oCDs for Cu^{2+} is evaluated under optimal conditions. Figure 5 shows the fluorescence spectra of Sc-oCDs after adding Cu^{2+} at various concentrations. At 558 nm, the fluorescence intensity of Sc-oCDs shows a gradual decrease alongside a rise in Cu^{2+} concentration. The Sc-oCDs solution undergoes a color change from bright

yellow to faint yellow as the Cu^{2+} concentration increased (inset of Figure 5). In the concentration range of 1–600 μM, a favorable linear correlation between F_0/F and C_{Cu2+} is observed, where the correlation coefficient reaches 0.99931. The linear regression equation is $F_0/F = 0.0206C + 0.9701$. The limit of detection (LOD) is determined using the formula $3\sigma/k$, where σ represents the standard deviation of blank measurements and k demotes the slope of the calibration curve. This is a theoretical LOD based on the instrument noise level, which is one of the most commonly used methods in spectroscopic techniques. The LOD achieved in this paper is 0.167 μM, that is to say, 0.011 ppm. The US EPA regulates the maximum limit of copper ions in drinking water at 1.3 ppm, the WHO sets it at 2.0 ppm, and China's standard is 1.0 ppm. In comparison, the detection limit in this study is fully capable of meeting these requirements for copper ion detection in drinking water.

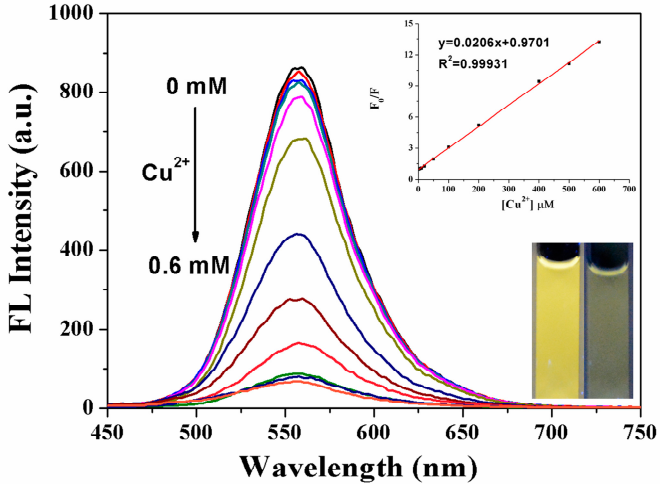


Figure 5. Fluorescent emission spectra of Sc-oCDs with the introduction of Cu^{2+} at various concentrations (from top to bottom, 0, 1, 2, 10, 20, 50, 100, 200, 300, 400, 500, and 600 μM). The inset images illustrate two key details: the upper one is the dependence of F_0/F on Cu^{2+} concentration over the range of 1–600 μM, while the inset image below shows photographs of the Sc-oCDs solutions under 365 nm UV light, with color shifting from bright yellow (without Cu^{2+}) to faint yellow (with 600 μM Cu^{2+}).

3.5. Selectivity of Sc-oCDs in Cu^{2+} Detection

Anti-interference capabilities are crucial for a sensor. Thus, we investigate the selectivity and competition of Sc-oCDs in Cu^{2+} detection (Figure S4). After adding different metal ion solution (such as Mn^{2+}, Mg^{2+}, Ba^{2+}, Cd^{2+},Co^{2+}, Al^{3+}, Zn^{2+}, Cr^{3+}, Fe^{3+}, Ni^{2+}, and Fe^{2+}) to the system, the fluorescence quenching values (F/F_0) of Sc-oCDs (600 μM) show no obvious changes. Their quenching effects are negligible compared with Cu^{2+}. This high selectivity may result from the stronger binding affinity of Sc-oCDs for Cu^{2+} in acidic media. These results confirm that the proposed fluorescence sensor exhibits high selectivity for Cu^{2+} compared to other metal ions, indicating Sc-oCDs have substantial potential for applications in real samples.

3.6. Possible Quenching Mechanism of Sc-oCDs by Cu^{2+}

Generally, fluorescence quenching may result from the dynamic quenching effect (DQE), static quenching effect (SQE), or their combination [56]. To explore how Cu^{2+}-induced fluorescence quenching in Sc-oCDs, further experiments are conducted. The quenching effect typically follows the Stern–Volmer equation [57]: $F_0/F = 1 + K_S[Q]$, where F_0 and F are the steady-state fluorescence intensities at 558 nm without and with Cu^{2+}, respectively; K_S is the Stern–Volmer constant, and [Q] denotes the concentration of quencher (Cu^{2+}). The linear relationship in Figure 5 confirms the equation's applicability. However, both DQE and SQE comply with the Stern–Volmer equation, making them

indistinguishable via this equation alone. For a deeper understanding of the fluorescence quenching mechanism, time-resolved fluorescence measurements are performed to identify the specific type of quenching involved. Figure 6A shows that the fluorescence decay of Sc-oCDs could be deconvoluted using a biexponential decay function. Given the relatively homogeneous nature of the Sc-oCDs, the intensity-weighted method was selected in the software for fitting to calculate the average fluorescence lifetime. Sc-oCDs have an average fluorescence lifetime of 4.14 ns (black line). With the addition of Cu^{2+}, the lifetime drops to 3.14 ns (red line). The significant reduction in average fluorescence lifetime demonstrates the occurrence of dynamic quenching. Additionally, UV-vis absorption spectra of the Sc-oCDs solution are recorded prior to and following the addition of Cu^{2+}. The absorption peak of Sc-oCDs remains unchanged following the addition of Cu^{2+}, as shown in Figure 6B, indicating the absence of new substances formation. While this observation does not preclude aggregation or non-covalent interactions, the decrease in fluorescence lifetime collectively confirms that dynamic quenching [58], rather than static quenching, occurs between the carbon dots and Cu^{2+}.

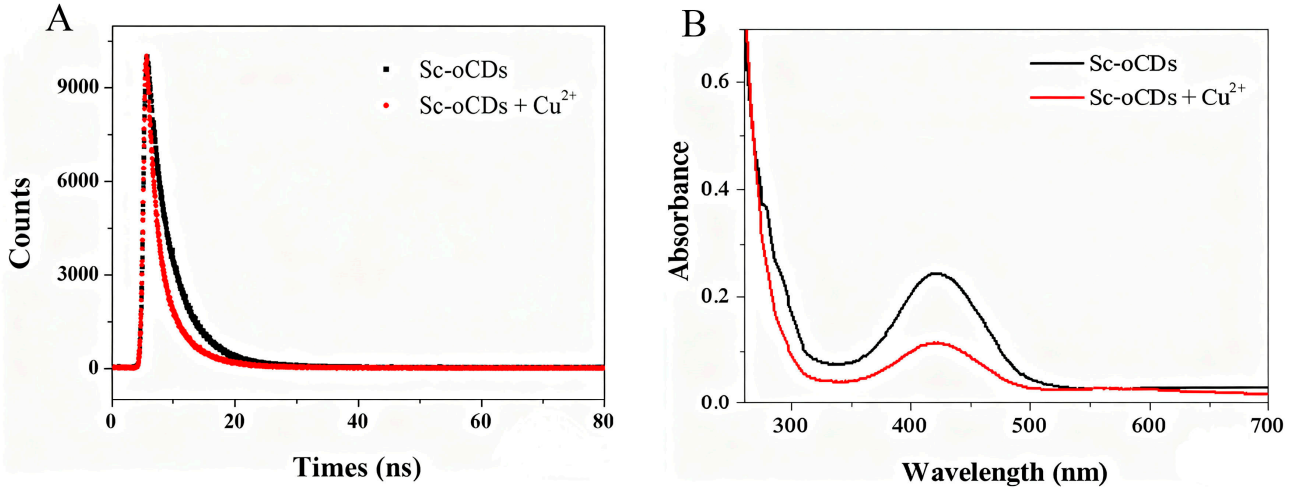


Figure 6. (**A**) Time-resolved decays (420 nm excitation) and (**B**) UV–vis absorption spectra of Sc-oCDs with (red line) and without (black line) Cu^{2+}.

3.7. Real Application

Finally, the prepared Sc-oCDs are applied as a sensor to detect Cu^{2+} in Yellow River water and tap water, with both results showing no detection. To further verify the accuracy of this method, Cu^{2+} in water samples is determined via the standard addition method, with the results presented in Table 1. The detection recoveries are found to range from 98.2% to 106.1%, with relative standard deviation (RSD) of 0.13% to 3.8% across three parallel experiments. Such results confirm the method's applicability for Cu^{2+} determination in actual samples. It is worth noting that the RSD of tap water is higher than that of Yellow River water. This can be attributed to the simpler matrix of tap water, rendering it more susceptible to pH variations and instrumental signal fluctuations in the reaction system. Residual chlorine and disinfection by-products in tap water may also compromise fluorescence intensity stability. In contrast, the complex composition of river water [59] diminishes the impact of matrix viscosity and homogeneity on operational variability. Additionally, the application of this upconversion material for Cu^{2+} detection in live HeLa cells was also investigated. However, the material was found to compromise cell viability. Therefore, we are currently modifying the material to endow it with biocompatibility and further develop its application potential in biological samples.

Table 1. Analytical results for the detection of Cu^{2+} in water samples.

Sample	Detected (μM)	Found (μM)	Recovery (%)	RSD [a] (%, *n* = 3)
Yellow river	20.0	19.7	98.6	0.14
	80.0	84.9	106.1	1.3
	320.0	321.9	100.6	0.13
Tap water	20.0	20.8	104.0	3.8
	80.0	82.8	103.5	1.9
	320.0	314.2	98.2	3.5

[a] The RSD values are derived from a set of three recovery data points.

For the detection of Cu^{2+} in water samples, the performance of the present work was benchmarked against existing approaches (Table 2). The solid-phase synthesis method, which produces Sc-oCDs after a mere 2 h reaction at 120 °C, offers markedly lower energy consumption due to its mild conditions. The process utilizes only centrifugation and dialysis for purification. Compared with solution-phase synthesis methods such as the solvothermal method, the solid-phase synthesis method requires very little organic reagent and does not generate a large amount of waste liquid, underscoring its potential for scalable production. In practical terms for water sample analysis, the material enables rapid detection of Cu^{2+}, with immediate signal stabilization within one minute without any incubation step. Table 2 also compares previously reported CDs for Cu^{2+} detection, listed in order of increasing LOD from 0.0023 μM to 4.7 μM [60–68]. Although the detection limit of the present method is not the lowest reported, it is well below the WHO guideline value of 31.2 μM for copper in drinking water, confirming its practical adequacy for compliance monitoring. With the advantages of low energy consumption and rapid response, the method reported in this paper is of great practical application value in the detection of actual water samples.

Table 2. Analytical performance comparison of various QDs for sensing of Cu^{2+} in water samples.

Carbon Dots	Synthesis Method	Synthesis Conditions	Response Time	Detection Limits (μM)	Applications	Ref.
NCDs	Solid-state pyrolytic method	200 °C to 300 °C, 1 h	5 min	0.0023	Tap water	[60]
QDs@Cu NCs	Copper nanoclusters conjugated to silica coated CdSe quantum dots (QDs)	Room temperature, >12 h	37 °C for 10 min	0.0089	River water, well water, industrial sewage	[61]
S-C-Dots	Base-catalyzed synthesis method	Room temperature, 12 h	/	0.052	/	[62]
Red dual-emissive CDs	Solid-phase synthesis	200 °C, 12 h	/	0.145	Tap water, seawater	[29]
Sc-oCDs	Solid-phase synthesis	120 °C, 2 h	1 min	0.167	River water and tap water	This work
BP/NS-CDs	Hydrothermal method	180 °C, 12 h	/	0.18	Tap and lake water	[63]
4-ASA/GdCDs	Hydrothermal method	200 °C, 3 h	2 min	0.23	Tap water	[22]
R-CDs	Hydrothermal method	180 °C, 10 h	/	0.58	Tap water, river water, seawater	[64]
AuNCs/CQDs	Hydrothermal synthesis	200 °C, 12 h	4 min	0.65	Tap water and lake water	[65]
B&Y-CQDs	Hydrothermal method	180 °C, 12 h	/	0.73	Tap water and rice samples	[66]
N-L-Ser-CDs	Solid-state pyrolysis method	180 °C, 2 h	5 min	3	/	[67]
N,S-CQDs	Hydrothermal method	150 °C, 4 h	/	4.7	Deionized water and tap water	[68]

4. Conclusions

This study reported the preparation of Sc-oCDs using a facile solid-phase synthetic method. The as-obtained Sc-oCDs was spherical with an average particle size of around 6.0 ± 1.2 nm. Optimal excitation at 420 nm and emission at 558 nm were observed for these Sc-oCDs, accompanied by remarkable optical stability against fluctuations in acidity, ionic strength, and photobleaching. Notably, the introduction of Sc not only enhanced the fluorescence quantum yield but also conferred upconversion properties (excitation: 980 nm; emission: 540 nm). Moreover, the synthesized Sc-oCDs were employed as a sensor for Cu^{2+} detection with a linear detection range of 1–600 μM (LOD: 0.167 μM) under optimal conditions. The detection mechanism was dynamic quenching. The method was effectively applied to real water samples, achieving satisfactory recovery rates, which confirms its practical value for water sample monitoring. The material exhibits both upconversion and downconversion luminescence; however, its effectiveness in cellular imaging is currently constrained. The limited amount of Sc, compounded by the unclear mechanism of action, also presents a constraint in this study. Overcoming these limitations is an important objective for our subsequent research.

Supplementary Materials: The following supporting information can be downloaded at: https://www.mdpi.com/article/10.3390/chemosensors13120430/s1, Figure S1: EDS analysis (A) and element mapping (B) of C (C) and Sc(D) for Sc-oCDs. The Sc-oCDs aggregated after being dropped from uniform solution onto the silicon wafer and dried, with a portion forming microspheres with a particle size greater than 2.5 μm; Figure S2: Fluorescence responses of Sc-oCDs toward (A) pH, (B) concentrations of NaCl and (C) light illumination (λ_{ex} = 420 nm); Figure S3: The effect of (A) various buffer solution (10 mM, pH 4.8), (B) pH and (C) reaction time on the fluorescence intensity of Sc-oCDs with the addition of Cu^{2+} at room temperature ([Cu^{2+}] = 600 μM); Figure S4: Fluorescence quenching values (F/F_0) of Sc-oCDs in the presence and absence of different metal ions (600 μM).

Author Contributions: Y.D.: conceptualization, formal analysis, investigation and writing—original draft; W.S.: methodology, investigation, formal analysis and validation; J.H.: methodology, resources and writing—review and editing; C.R.: funding acquisition, resources and supervision. All authors have read and agreed to the published version of the manuscript.

Funding: This research was financially supported by the National Natural Science Foundation of China (No. 21874061) and the Science and Technology program of Gansu Province (No. 22JR5RA476).

Data Availability Statement: Data will be made available on request.

Conflicts of Interest: The authors declare that they have no conflicts of interest.

References

1. Yousaf, A.; Imran, M.; Warsi, M.F.; Alsafari, I.A.; Khan, F.A.; Parra-Saldívar, R.; Gutiérrez-Soto, G.; Iqbal, H.M.N. Nanomaterials as a new frontier platform: Metal-doped and hybrid carbon dots as enzyme mimics for environmental applications. *Front. Mater.* **2025**, *12*, 116583. [CrossRef]
2. Yang, H.-L.; Bai, L.-F.; Geng, Z.-R.; Chen, H.; Xu, L.-T.; Xie, Y.-C.; Wang, D.-J.; Gu, H.-W.; Wang, X.-M. Carbon quantum dots: Preparation, optical properties, and biomedical applications. *Mater. Today Adv.* **2023**, *18*, 100376. [CrossRef]
3. Namdari, P.; Negahdar, B.; Eatemadi, A. Synthesis, properties and biomedical applications of carbon-based quantum dots: An updated review. *Biomed. Pharmacother.* **2017**, *87*, 209–222. [CrossRef] [PubMed]
4. Wang, Z.; Changotra, R.; Dasog, M.; Selopal, G.S.; Yang, J.; He, Q.S. Carbon quantum dots: Synthesis via hydrothermal processing, doping strategies, integration with photocatalysts, and their application in photocatalytic hydrogen production. *Sustain. Mater. Technol.* **2025**, *44*, e01386. [CrossRef]
5. Rani, G.; Siddharth; Ahlawat, R.; Kumar, H. A Comprehensive review on the Synthesis, doping, and characterization techniques of carbon quantum dots for their multifaceted applications. *Comments Inorg. Chem.* **2025**, *45*, 172–209. [CrossRef]
6. Abbasi, A.; Shakir, M. Simple One-step solid-state synthesis of highly crystalline N doped carbon dots as selective turn off-sensor for picric acid and metanil yellow. *J. Fluoresc.* **2022**, *32*, 1239–1246. [CrossRef]

7. Li, C.; Li, N.; Yang, L.; Liu, L.; Zhang, D. Synthesis of fluorescent carbon dots by B/P doping and application for Co^{2+} and methylene blue detection. *Spectrochim. Acta Part A Mol. Biomol. Spectrosc.* **2024**, *309*, 123824. [CrossRef]
8. Jian, K.; Men, W.; Miao, C.; Du, Y.; Yang, H.; Zhao, X. Fe-doped carbon dots with enhanced fluorescence: Facilitating Cu^{2+} detection and urea electro-oxidation. *Talanta* **2025**, *292*, 127942. [CrossRef]
9. Gopi, P.; Ponnusamy, K. Influence of magnesium doping on carbon dots for enhancing photocurrent generation in photodetectors. *Phys. Scr.* **2025**, *100*, 035944. [CrossRef]
10. Gao, W.; Hu, H.; Xue, J.; Dong, Y.; Li, W.; Zhao, X.; Mao, Z.; Li, Z. F and Na Co-doped carbon dots with enhanced afterglow emission for applications in fingerprint recognition and information encryption. *Spectrochim. Acta Part A Mol. Biomol. Spectrosc.* **2025**, *339*, 126259. [CrossRef] [PubMed]
11. Yashwanth, H.J.; Naik, M.M.; Dileep, M.S.; Muniyappa, M.; Rani, M.N. Nitrogen, phosphorous co-doped carbon quantum dots as glucose and lactate sensor. *Mater. Chem. Phys.* **2025**, *331*, 130149. [CrossRef]
12. Chien, Y.-H.; Chan, K.K.; Yap, S.H.K.; Yong, K.-T. NIR-responsive nanomaterials and their applications; upconversion nanoparticles and carbon dots: A perspective. *J. Chem. Technol. Biotechnol.* **2018**, *93*, 1519–1528. [CrossRef]
13. Cheisson, T.; Schelter, E.J. Rare earth elements: Mendelee's bane, modern marvels. *Science* **2019**, *363*, 489–493. [CrossRef]
14. Zhang, M.; Zhai, X.; Sun, M.; Ma, T.; Huang, Y.; Huang, B.; Du, Y.; Yan, C. When rare earth meets carbon nanodots: Mechanisms, applications and outlook. *Chem. Soc. Rev.* **2020**, *49*, 9220–9248. [CrossRef] [PubMed]
15. da Rocha, J.D.G.; Cechinel, M.A.P.; Rocha, L.F.; Riella, H.G.; Padoin, N.; Soares, C. Exploring the potential of rare earth doped carbon dots: Concepts and applications. *Chem. Eng. J. Adv.* **2024**, *17*, 100583. [CrossRef]
16. Wang, Y.; Hong, F.; Yu, L.; Xu, H.; Liu, G.; Dong, X.; Yu, W.; Wang, J. Construction, energy transfer, tunable multicolor and luminescence enhancement of YF_3: RE^{3+} (RE=Eu, Tb)/carbon dots nanocomposites. *J. Luminesc.* **2020**, *221*, 117072. [CrossRef]
17. Zhang, Z.; Li, J.; Wang, X.; Liang, A.; Jiang, Z. Aptamer-mediated N/Ce-doped carbon dots as a fluorescent and resonance Rayleigh scattering dual mode probe for arsenic(III). *Microchim. Acta* **2019**, *186*, 638. [CrossRef]
18. Zhang, M.; Wang, W.; Yuan, P.; Chi, C.; Zhang, J.; Zhou, N. Synthesis of lanthanum doped carbon dots for detection of mercury ion, multi-color imaging of cells and tissue, and bacteriostasis. *Chem. Eng. J.* **2017**, *330*, 1137–1147. [CrossRef]
19. Shi, Y.; Xia, Y.; Zhou, M.; Wang, Y.; Bao, J.; Zhang, Y.; Cheng, J. Facile synthesis of Gd/Ru-doped fluorescent carbon dots for fluorescent/MR bimodal imaging and tumor therapy. *J. Nanobiotechnol.* **2024**, *22*, 88. [CrossRef] [PubMed]
20. Chu, H.; Yao, D.; Chen, J.; Yu, M.; Su, L. Detection of Hg^{2+} by a dual-fluorescence ratio probe constructed with rare-earth-element-doped cadmium telluride quantum dots and fluorescent carbon dots. *ACS Omega* **2021**, *6*, 10735–10744. [CrossRef] [PubMed]
21. Zhang, T.; Zhai, Y.; Wang, H.; Zhu, J.; Xu, L.; Dong, B.; Song, H. Facilely prepared carbon dots and rare earth ion doped hybrid composites for ratiometric pH sensing and white-light emission. *RSC Adv.* **2016**, *6*, 61468–61472. [CrossRef]
22. Zhao, D.; Zhang, C.; Liu, H.; Jiao, Y.; Xiao, X. Gadolinium-doped carbon dots with dual enzyme activity for visual detection of Cu^{2+} and antibacterial applications. *ACS Appl. Nano Mater.* **2024**, *7*, 4228–4238. [CrossRef]
23. Sun, Z.; Li, H.; Pittman, A.S.; Cao, Y. Scandium detection of carbon dot based on bottom-up hydrothermal synthesis. *Ceram. Int.* **2025**, *51*, 16923–16935. [CrossRef]
24. Chen, X.; Lin, Y.; Liao, J.; Zhang, J.; Zheng, C. Light-activated carbon dot nanozyme with scandium for a highly efficient and pH-universal bio-nanozyme cascade colorimetric assay. *J. Mater. Chem. B* **2023**, *11*, 6697–6703. [CrossRef]
25. Yang, J.; Li, P.; Song, Z.; Li, J.; Yang, H.; Yan, F.; Li, L.; Xu, C.; Chen, J.; Chen, L. Graphene quantum dots via ion modification for improving photoluminescence stability in aqueous solution with heavy metal ions. *Appl. Surf. Sci.* **2022**, *593*, 153367. [CrossRef]
26. Ren, H.; Qi, F.; Feng, X.; Liu, J.; Zhao, Y. Facile synthesis of fluorescent carbon quantum dots with high product yield using a solid-phase strategy. *Molecules* **2024**, *29*, 5317. [CrossRef]
27. Zhao, D.; Zhang, Z.; Li, C.; Xiao, X.; Li, J.; Liu, X.; Cheng, H. Yellow-emitting hydrophobic carbon dots via solid-phase synthesis and their applications. *ACS Omega* **2020**, *5*, 22587–22595. [CrossRef]
28. Ji, X.; Xu, Y.; Wang, Z.; Huang, X.; Xiao, G.; Yang, G.; Feng, W. One-step synthesis of N-doped carbon dots as sensitive "on-off-on" fluorescent sensor for tetracycline and Al^{3+} detection. *Microchem. J.* **2023**, *185*, 108290. [CrossRef]
29. Yang, F.; Zhou, P.; Duan, C. Solid-phase synthesis of red dual-emissive nitrogen-doped carbon dots for the detection of Cu^{2+} and glutathione. *Microchem. J.* **2021**, *169*, 106534. [CrossRef]
30. Dang, D.K.; Chandrasekaran, S.; Ngo, Y.-L.T.; Chung, J.S.; Kim, E.J.; Hur, S.H. One pot solid-state synthesis of highly fluorescent N and S co-doped carbon dots and its use as fluorescent probe for Ag^{+} detection in aqueous solution. *Sens. Actuators B Chem.* **2018**, *255*, 3284–3291. [CrossRef]
31. Wei, H.; Li, H.; Zhang, Y.; Wang, X.; Li, Z.; Zhou, M.; Lei, Y.; Guo, P.; Liu, J.; Yang, S. Solid-phase synthesized iron-mediated carbon dots nanozymes with fluorescence and peroxidase-like activity for multi-mode analysis of dopamine. *Microchem. J.* **2025**, *208*, 112597. [CrossRef]
32. Taylor, A.A.; Tsuji, J.S.; Garry, M.R.; McArdle, M.E.; Goodfellow, W.L., Jr.; Adams, W.J.; Menzie, C.A. Critical review of exposure and effects: Implications for setting regulatory health criteria for ingested copper. *Environ. Manag.* **2020**, *65*, 131–159. [CrossRef]

33. Bisaglia, M.; Bubacco, L. Copper Ions and Parkinson's Disease: Why Is Homeostasis So Relevant? *Biomolecules* **2020**, *10*, 195. [CrossRef] [PubMed]
34. Odetola, L.; Sills, S.; Morrison, S. A pilot study on the feasibility of testing residential tap water in North Carolina: Implications for environmental justice and health. *J. Expo. Sci. Environ. Epidemiol.* **2021**, *31*, 972–978. [CrossRef] [PubMed]
35. Bagherian, G.; Chamjangali, M.A.; Evari, H.S.; Ashrafi, M. Determination of copper(II) by flame atomic absorption spectrometry after its preconcentration by a highly selective and environmentally friendly dispersive liquid–liquid microextraction technique. *J. Anal. Sci. Technol.* **2019**, *10*, 3. [CrossRef]
36. Venkatesan, A.K.; Rodríguez, B.T.; Marcotte, A.R.; Bi, X.; Schoepf, J.; Ranville, J.F.; Herckes, P.; Westerhoff, P. Using single particle ICP-MS for monitoring metal-containing particles in tap waters. *Environ. Sci. Water Res. Technol.* **2018**, *4*, 1923–1932. [CrossRef]
37. Gerdan, Z.; Saylan, Y.; Denizli, A. Recent advances of optical sensors for copper ion detection. *Micromachines* **2022**, *13*, 1298. [CrossRef]
38. Romero-Cano, L.A.; Zárate-Guzmán, A.I.; Carrasco-Marín, F.; González-Gutiérrez, L.V. Electrochemical detection of copper in water using carbon paste electrodes prepared from bio-template (grapefruit peels) functionalized with carboxyl groups. *J. Electroanal. Chem.* **2019**, *837*, 22–29. [CrossRef]
39. Rekhi, H.; Rani, S.; Sharma, N.; Malik, A.K. A Review on Recent Applications of High-Performance Liquid Chromatography in Metal Determination and Speciation Analysis. *Crit. Rev. Anal. Chem.* **2017**, *47*, 524–537. [CrossRef]
40. *GB 5009.94-2012*; National Food Safety Standard-Determination of Rare Earth Elements in Plant-Derived Foods. Ministry of Health of the People's Republic of China: Beijing, China, 2012.
41. Zhang, H.; Chen, Y.; Liang, M.; Xu, L.; Qi, S.; Chen, H.; Chen, X. Solid-phase synthesis of highly fluorescent nitrogen-doped carbon dots for sensitive and selective probing ferric ions in living cells. *Anal. Chem.* **2014**, *86*, 9846–9852. [CrossRef] [PubMed]
42. Wu, F.; Su, H.; Zhu, X.; Wang, K.; Zhang, Z.; Wong, W.-K. Near-infrared emissive lanthanide hybridized carbon quantum dots for bioimaging applications. *J. Mater. Chem. B* **2016**, *4*, 6366–6372. [CrossRef]
43. Liu, Y.; Zhou, L.; Li, Y.; Deng, R.; Zhang, H. Highly fluorescent nitrogen-doped carbon dots with excellent thermal and photo stability applied as invisible ink for loading important information and anti-counterfeiting. *Nanoscale* **2017**, *9*, 491–496. [CrossRef] [PubMed]
44. Zhang, M.; Su, R.; Zhong, J.; Fei, L.; Cai, W.; Guan, Q.; Li, W.; Li, N.; Chen, Y.; Cai, L.; et al. Red/orange dual-emissive carbon dots for pH sensing and cell imaging. *Nano Res.* **2019**, *12*, 815–821. [CrossRef]
45. Hao, Y.; Song, Y.; Li, T.; Tuo, Y.; Tian, M.; Chai, F. Controllable synthesis of yellow emissive carbon dots by mild heating process and their utility as fluorescent test paper for detection of mercury (II) ions assistants by smartphone. *J. Environ. Chem. Eng.* **2023**, *11*, 109863. [CrossRef]
46. Liao, H.; Wang, Z.Y.; Chen, S.; Wu, H.; Ma, X.J.; Tan, M.Q. One-pot synthesis of gadolinium(III) doped carbon dots for fluorescence/magnetic resonance bimodal imaging. *RSC Adv.* **2015**, *5*, 66575. [CrossRef]
47. Dewangan, L.; Chawre, Y.; Korram, J.; Karbhal, I.; Nagwanshi, R.; Jain, V.; Satnami, M.L. N-doped, silver, and cerium co-doped carbon quantum dots based sensor for detection of Hg^{2+} and captopril. *Microchem. J.* **2022**, *182*, 107867. [CrossRef]
48. Wang, H.P.; Xing, H.Z.; Liu, W.; Hao, Y.M.; Zhang, L.; Yang, Z.H.; Hu, Q.; Shuang, S.M.; Dong, C.; Gong, X.J. Gadolinium-doped carbon dots as a ratiometric fluorometry and colorimetry dual-mode nano-sensor based on specific chelation for morin detection. *Sens. Actuators B Chem.* **2022**, *352*, 130991. [CrossRef]
49. Yang, Z.; Xu, M.; Liu, Y.; He, F.; Gao, F.; Su, Y.; Wei, H.; Zhang, Y. Nitrogen-doped, carbon-rich, highly photoluminescent carbon dots from ammonium citrate. *Nanoscale* **2014**, *6*, 1890–1895. [CrossRef]
50. Würth, C.; Grabolle, M.; Pauli, J.; Spieles, M.; Resch-Genger, U. Relative and absolute determination of fluorescence quantum yields of transparent samples. *Nat. Protoc.* **2013**, *8*, 1535–1550. [CrossRef]
51. Li, Y.; Zhao, Y.; Cheng, H.; Hu, Y.; Shi, G.; Dai, L.; Qu, L. Nitrogen-doped graphene quantum dots with oxygen-rich functional groups. *J. Am. Chem. Soc.* **2012**, *134*, 15–18. [CrossRef]
52. Yang, Z.; Li, X.; Wang, J. Intrinsically fluorescent nitrogen-containing carbon nanoparticles synthesized by a hydrothermal process. *Carbon* **2011**, *49*, 5207–5212. [CrossRef]
53. Li, H.Q.; Wei, Z.N.; Zuo, X.W.; Chen, H.L.; Ren, C.L.; Dong, Y.L.; Chen, X.G. Carbon dots for real-time colorimetric/fluorescent dual-mode sensing ClO^-/GSH. *Dye. Pigment.* **2022**, *206*, 110614. [CrossRef]
54. Peng, H.; Travas-Sejdic, J. Simple aqueous solution route to luminescent carbogenic dots from carbohydrates. *Chem. Mater.* **2009**, *21*, 5563–5565. [CrossRef]
55. Zhu, S.; Zhang, J.; Liu, X.; Li, B.; Wang, X.; Tang, S.; Meng, Q.; Li, Y.; Shi, C.; Hu, R.; et al. Graphene quantum dots with controllable surface oxidation, tunable fluorescence and up-conversion emission. *RSC Adv.* **2012**, *2*, 2717–2720. [CrossRef]
56. Lakowicz, J.R. *Principles of Fluorescence Spectroscopy*, 3rd ed.; Kluwer Academic/Plenum Publishers: New York, NY, USA, 2006; ISBN 978-0-387-31278-1.
57. Zhai, W.; Wang, C.; Yu, P.; Wang, Y.; Mao, L. Single-layer MnO_2 nanosheets suppressed fluorescence of 7-hydroxycoumarin: Mechanistic study and application for sensitive sensing of ascorbic acid in vivo. *Anal. Chem.* **2014**, *86*, 12206–12213. [CrossRef]

58. Bai, Z.; Yan, F.; Xu, J.; Zhang, J.; Wei, J.; Luo, Y.; Chen, L. Dual-channel fluorescence detection of mercuric (II) and glutathione by down- and up-conversion fluorescence carbon dots. *Spectrochim. Acta Part A Mol. Biomol. Spectrosc.* **2018**, *205*, 29–39. [CrossRef]
59. Yu, Q.L.; Feng, T.S.; Yang, J.W.; Su, W.H.; Zhou, R.; Wang, Y.J.; Zhang, H.; Li, H. Seasonal distribution of antibiotic resistance genes in the Yellow River water and tap water, and their potential transmission from water to human. *Environ. Pollut.* **2022**, *292*, 118304. [CrossRef] [PubMed]
60. Patir, K.; Gogoi, S.K. Nitrogen-doped carbon dots as fluorescence ON–OFF–ON sensor for parallel detection of copper(II) and mercury(II) ions in solutions as well as in filter paper-based microfluidic device. *Nanoscale Adv.* **2019**, *1*, 592–601. [CrossRef]
61. Liu, Z.-C.; Qi, J.-W.; Hu, C.; Zhang, L.; Song, W.; Liang, R.-P.; Qiu, J.-D. Cu nanoclusters-based ratiometric fluorescence probe for ratiometric and visualization detection of copper ions. *Anal. Chim. Acta* **2015**, *895*, 95–103. [CrossRef]
62. Cardoso-Ávila, P.E.; Pichardo-Molina, J.L. Utilizing Chicken Egg White and L-Cysteine for Green Synthesis of Carbon Dots: Rapid and Cost-Effective Detection of Cu^{2+} Ions. *Materials* **2025**, *18*, 637. [CrossRef] [PubMed]
63. Sonaimuthu, M.; Ganesan, S.; Anand, S.; Jagadeesh Kumar, A.; Palanisamy, S.; You, S.G.; Velsankar, K.; Sudhahar, S.; Lo, H.-M.; Lee, Y.R. Multiple heteroatom dopant carbon dots as a novel photoluminescent probe for the sensitive detection of Cu^{2+} and Fe^{3+} ions in living cells and environmental sample analysis. *Environ. Res.* **2023**, *219*, 115106. [CrossRef]
64. Huang, S.; Mu, P.; Li, G.; Ni, W.; Fang, Y.; Wei, F.; Xiao, Q. Highly sensitive red-emitting carbon dot-based fluorescence sensor for simultaneous detection of copper ions and L-histidine in environmental and biomedical samples. *J. Photochem. Photobiol. A Chem.* **2025**, *469*, 116588. [CrossRef]
65. He, W.; Lim, S.F.; Baini, R.; Qu, Y.; Li, X. Visual determination of copper (II) using a biomass sourced carbon quantum dot (CQD) ratiometric fluorescent probe. *Anal. Lett.* **2025**, *58*, 228–241. [CrossRef]
66. Lu, H.; Yin, Y.; Zhao, Y.; Xing, X.; Zhang, Y.; Sun, C. A ratiometric and colorimetric dual-mode fluorescence method for the sensitive determination of copper ion. *Fuller. Nanotub. Carbon Nanostruct.* **2025**, *33*, 526–537. [CrossRef]
67. Yao, Z.; Wang, C.; Ma, Z.; Huang, R.; Wang, B.; Zhang, J.; Zhao, X.; Zhang, W.; Shi, H. Solid-phase pyrolysis synthesis of amino acid-based nitrogen-doped carbon dots as an "on-off-on" fluorescent probe for the detection of copper ions and glutathione. *J. Fluoresc.* **2025**, *35*, 8665–8676. [CrossRef] [PubMed]
68. Chaudhary, N.; Gupta, P.K.; Eremin, S.; Solanki, P.R. One-step green approach to synthesize highly fluorescent carbon quantum dots from banana juice for selective detection of copper ions. *J. Environ. Chem. Eng.* **2020**, *8*, 103720. [CrossRef]

Disclaimer/Publisher's Note: The statements, opinions and data contained in all publications are solely those of the individual author(s) and contributor(s) and not of MDPI and/or the editor(s). MDPI and/or the editor(s) disclaim responsibility for any injury to people or property resulting from any ideas, methods, instructions or products referred to in the content.